Letters

Experimental Study on Static and Dynamic Characteristics of Ga_2O_3 Schottky Barrier Diodes With Compound Termination

Yuxi Wei, Xiaorong Luo, Yuangang Wang, Juan Lu, Zhuolin Jiang, Jie Wei, Yuanjie Lv, and Zhihong Feng

***Abstract*—In this letter, the ultrafast reverse recovery β-Ga_2O_3 Schottky barrier diode (SBD) with improved breakdown voltage is proposed and investigated experimentally. It features the compound termination, consisting of air space field plate and thermal oxidation terminal. The compound termination not only reduces high-density interface states at the dielectric/Ga_2O_3 interface and the electron concentration in the oxidation terminal, but also modulates the electric-field distribution and suppresses the peak electric-field at the bottom of anode. Therefore, the reverse leakage current is suppressed as well as the reverse recovery and breakdown characteristics are improved effectively. The Ga_2O_3 SBDs with the diameter of 1000 μm obtain ultrashort reverse recovery time of 7.5 ns and ultralow reverse recovery charge of 1.0 nC at *di/dt* = 50 A/μs with its breakdown voltage up to 400 V, maintaining good rectification characteristics. The temperature-dependences of both forward conduction and reverse recovery characteristics are discussed in temperature range from 300 to 500 K. The results prove that the superior electronics performance of the β-Ga_2O_3 SBDs with good electronics thermal tolerance can overcome the low thermal conductivity of β-Ga_2O_3 to a certain extent. The fabricated β-Ga_2O_3 SBDs have great potential for high power and high-frequency applications.**

***Index Terms*—Dynamic characteristic, gallium oxide (Ga_2O_3), reverse recovery, schottky barrier diode, temperature dependence.**

I. Introduction

With an ultrawide bandgap (E_g) and high breakdown electric field (E-field), the Baliga's figure of merit (more than 3000) of β-Ga_2O_3 is theoretical approximate 4 times and 10 times as large as that value of GaN and SiC, respectively [1]. Thus, β-Ga_2O_3 power devices have smaller size and lower loss at the same breakdown voltage (*BV*), and are expected to be sufficiently robust to operate under extremely severe conditions. The low-cost growth technology of large diameter and high-quality single-crystal β-Ga_2O_3 bulk substrates provides an additional advantage in the device production and application [2], [3]. As unipolar devices, Schottky barrier diodes (SBDs) have high switching speed and high reverse recovery performance**.** Combining the superior performance of the SBD with excellent material property, when the β-Ga_2O_3 SBDs are used for switching, freewheeling, and rectification in power conversion systems, the conversion efficiency and power density of the system can significantly be improved.

Many research works on electrical characteristics of β-Ga_2O_3 SBD with an improved termination have been reported. Both of ion-implantation [4]–[6] and field-plate [6], [7] are common termination to improve static characteristics, in which Hu *et al.* [6] combines the two termination but it requires additional process steps. Further study on large-size Ga_2O_3 SBDs with the diameter (D) of 1500 and 500 μm [8] have reported the *BV* of 300 V and 427 V, with the specific ON-resistance ($R_{on,sp}$) of 60 mΩ·cm^2 and 14.3 mΩ·cm^2, respectively. The dynamic characteristics of Ga_2O_3 rectifiers have been studied with the decreased reverse recovery time (T_{rr}) of $<$ 20 ns [4], [9]–[11]. The optimized 100-μm-diameter Ga_2O_3 SBD with ion-implanted planar edge termination [4] showed T_{rr} of 14.1 ns with the *BV* of 391 V and $R_{on,sp}$ of 4 mΩ·cm^2. In addition, the field-plated edge-terminated Schottky rectifiers with large area of 1 mm diameter [12] achieved T_{rr} of 64 ns in test circuit. In addition to the high voltage/current capability in high-power applications, the dynamic performance for the large-size Ga_2O_3 SBDs is of fundamental importance in high-efficiency fast switching applications.

In this work, the static and dynamic characteristics of β-Ga_2O_3 compound termination (CT) SBDs with the diameter of 1000 μm are studied experimentally. With $BV = 400$ V and $R_{on,sp} = 4$ mΩ·cm^2, the large size β-Ga_2O_3 CT SBD shows ultrashort T_{rr} and ultralow reverse recovery charge (Q_{rr}).

II. Experiments

The schematic cross section of the proposed vertical β-Ga_2O_3 SBDs with the CT is shown in Fig. 1(a). The CT consists of

Manuscript received January 17, 2021; revised February 18, 2021 and March 15, 2021; accepted March 27, 2021. Date of publication March 31, 2021; date of current version June 30, 2021. This work was supported by the Key Laboratory Fund Project under Grant 2020F2606003. *(Corresponding authors: Xiaorong Luo and Zhihong Feng.)*

Yuxi Wei, Xiaorong Luo, Juan Lu, Zhuolin Jiang, and Jie Wei are with the State Key Laboratory of Electronic Thin Films and Integrated Devices, University of Electronic Science and Technology of China, Chengdu 610054, China (e-mail: yuxi.wei@foxmail.com; xrluo@uestc.edu.cn; lujuanstu@163.com; jiangzhuolinee@163.com; weijieuestc@uestc.edu.cn).

Yuangang Wang, Yuanjie Lv, and Zhihong Feng are with the National Key Laboratory of Application Specific Integrated Circuit, Hebei Semiconductor Research Institute, Hebei 050051, China (e-mail: wyg123006@126.com; yuanjielv@163.com; ga917vv@163.com).

Color versions of one or more figures in this article are available at https://doi.org/10.1109/TPEL.2021.3069918.

Digital Object Identifier 10.1109/TPEL.2021.3069918

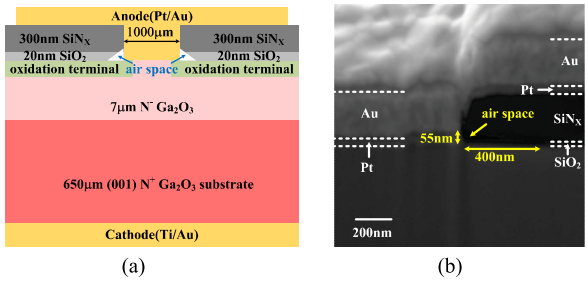

Fig. 1. (a) Schematic cross-section of Ga_2O_3 CT SBD. (b) SEM image of the fabricated Ga_2O_3 SBD.

thermal oxidation terminal and air space field plate (ASFP). It is fabricated on a 650-μm n-type (0 0 1)-oriented native substrate. The oxidation terminal is formed by the thermal oxidation annealing at 400 °C in an O_2 atmosphere for 30 min. It thus reduces the interface states by passivating the oxygen-vacancy type surface states and compensating surface charges, and thus increases the electron tunneling width [13]. Meanwhile, the oxidation terminal modulates the E-field distribution and suppresses the peak E-field [14]. The ASFP is composed of the air space and metal field plate. In Fig. 1(a) and (b), the air space is formed near the bottom of the anode since the wet etching (BOE: H_2O = 1:5, 60 s) rate of SiO_2 is faster than that of SiN_x. The deposition and annealing of cathode metal are implemented before wet etching, and there is no post annealing after anode metal deposition. The air space reduces interface states by removing the SiO_2/Ga_2O_3 interface with high density interface states. As a field plate, the ASFP not only induces a new E-field peak at air space edge [15], but also reduces E-field peak at anode to suppress the transmission coefficient and decrease the carrier tunneling rate [16]. Thus, both oxidation terminal and ASFP not only improve *BV*, but also reduce interface states, and thus suppress reverse leakage current, as well as improve the reverse recovery characteristics by decreasing charging/discharging of the interface states.

III. Results and Discussion

Fig. 2(a) shows the log-scale forward *J–V* characteristics of β-Ga_2O_3 CT SBD as a function of ambient temperatures (*T*). As *T* rises, the turn-ON voltage (V_{ON}) reduces from 0.7 to 0.4 V. The forward *J-V* curves at $T = 300$ K before and after 500 K temperature ramp almost are the same, which illustrates that short-term high-temperature will not influence the performance of the β-Ga_2O_3 SBDs. Fig. 2(b) shows the linear-scale forward *J–V* curves and $R_{on,sp}$ at different temperatures. At room temperature, the saturated output current is up to 400 A/cm^2 at forward bias of 2.5 V and $R_{on,sp} = 4$ mΩ·cm^2. Since the electron mobility decreases with the increasing temperature from 300 to 500 K, the slope of the curve decreases and $R_{on,sp}$ increases. According to the thermionic emission model [17], the ideality factor (*n*) and Schottky barrier height (φ_B) with *T* from 300 to 500 K are calculated as shown in Fig. 2(c), which are obtained by fitting the linear range of ln *J–V* plot. The extracted *n* is close to unity, and the values of *n* and φ_B are relatively

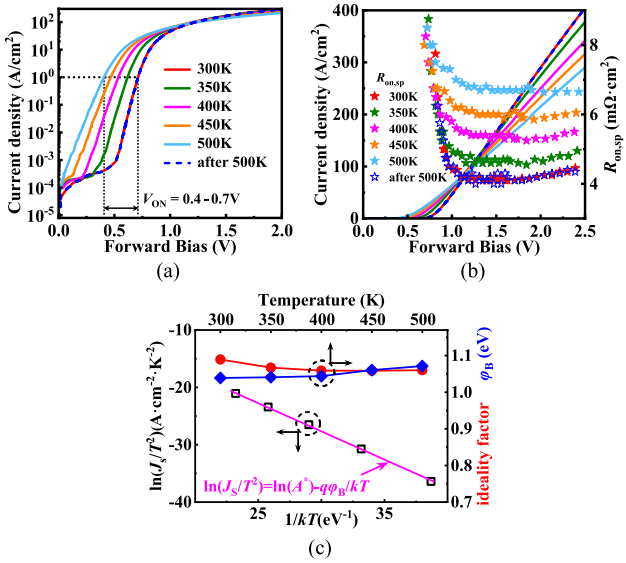

Fig. 2. (a) Log-scale and (b) linear-scale measured forward *J–V* characteristics as a function of temperature. (c) Temperature dependence of φ_B and *n*, and Richardson constant plot. The magenta line in (c) is the linear fit. The device was cooled down to the room temperature after each temperature step.

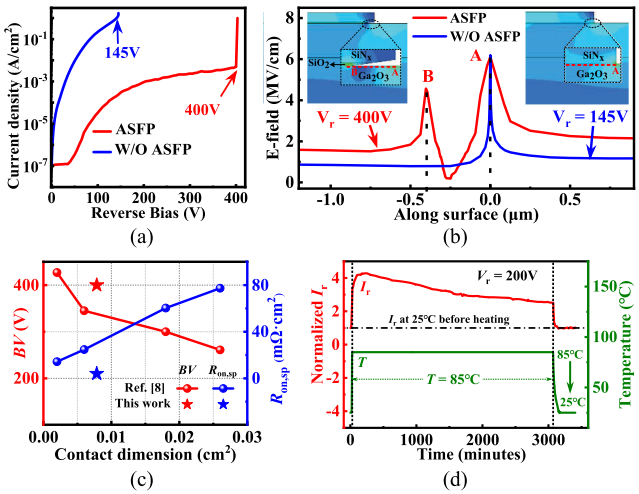

Fig. 3. (a) Measured reverse *J-V* characteristics. (b) Simulated E-field distribution under the surface of drift layer 1 nm (along the red dotted cut line in the insets). Points A and B represent the two edges of the air space. (c) Comparison of area-dependent *BV* and $R_{on,sp}$. (d) Thermal reliability test.

stable with little temperature-dependence. As the temperature increases, *n* decreases from 1.09 to 1.06 and φ_B increases from 1.04 to 1.07 eV, as shown in Fig. 2(c). This tendency of *n* and φ_B with temperature has been commonly observed in reported β-Ga_2O_3 and GaN SBDs, attributing to the Schottky barrier height inhomogeneity [17], [18]. According to the linear fit of the experimental data at different temperatures in Fig. 2(c), φ_B and A^* derived from the Richardson constant plot are 1.02 eV and 40.12 A·cm^{-2}·K^{-2}, being in well agreement with the value extracted from linear fit of ln*J-V* in Fig. 2(a) and the ideal value of the β-Ga_2O_3 material (41.1 A·cm^{-2}·K^{-2}), respectively.

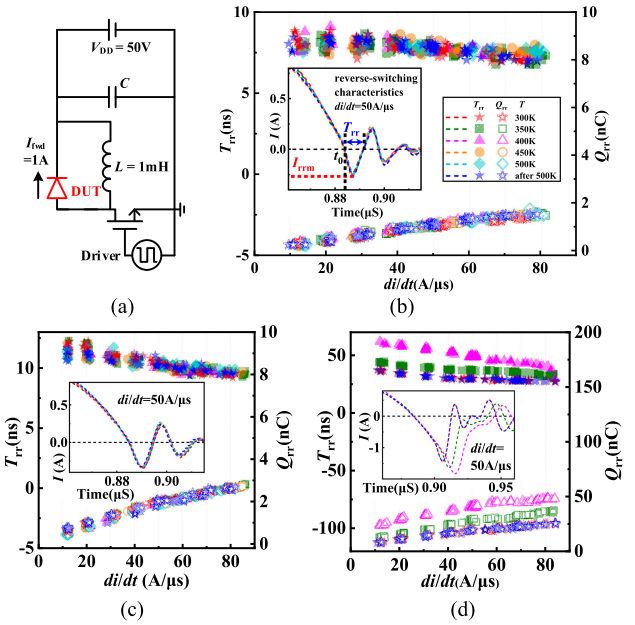

Fig. 4. (a) Switching circuit. Temperature dependence of T_{rr} and Q_{rr} for (b) Ga_2O_3 and (c) SiC SBDs, and (d) Si FRDs at temperatures ranging from 300 to 500 K and at 300 K again after 500 K temperature ramp. The inset shows reverse-switching curves at $di/dt = 50$ A/μs.

Fig. 3(a) shows the measured BV of the CT SBD up to 400 V, while the BV is only 145 V for the device without ASFP structure, which has a single SiN_x passivation layer with the same epitaxial layer as the Ga_2O_3 CT SBD. The two structures simulated by Sentaurus TCAD are shown in Fig. 3(b). The leakage current of the proposed large-size device remains at a low current density. The ASFP structure can not only suppress the reverse leakage current, but also modulate the electric field distribution. Fig. 3(b) shows the simulated E-field distribution. Inducing new peak E-field, the reverse bias (V_r) of the CT SBD is 400 V, improving greatly compared with $\sim$ 145 V of another structure with similar peak E-field at point A. Fig. 3(c) compares the area-dependent BV and $R_{on,sp}$ for the proposed CT SBD and the reported Ga_2O_3 SBD with single SiO_2 passivation and 11-μm-thick drift layer [8]. The CT SBD exhibits higher BV and lower $R_{on,sp}$ with the similar contact area, which means a larger Baliga's figure-of-merit (BFOM). With the thinner drift layer to achieve lower $R_{on,sp}$, the CT SBD shows larger BV, indicating that CT can effectively modulate the electric field distribution [see Fig. 3(b)] and suppress the reverse leakage current (I_r). Fig. 3(d) shows the I_r–V_r characteristics of the CT SBD at $T = 85$ °C and $V_r = 200$ V for 3000 min, which is normalized with I_r at $T = 25$ °C and $V_r = 200$ V so as to compare the influence of T on I_r. The tendency of I_r–V_r curve over time is similar to that in reported tests, and may be caused by charge relocation inside the devices [19], [20]. No major transient leakage is visible, and the measured I_r at T cooled down to 25 °C is almost the same as I_r before heating, validating the thermal reliability of the CT SBD.

Fig. 4 illustrates the temperature dependence of T_{rr} and Q_{rr} among the Ga_2O_3 SBD, the commercial SiC SBD (STPSC406, 600 V/4 A) [21] and Si fast recovery diode (FRD, SF36, 400 V/3 A) [22] at different di/dt before t_0. The value of di/dt is controlled by the external circuit and leads to an immediate impact on the peak reverse recovery current (I_{rrm}), while the values of di/dt after t_0 depend on the device performance itself. With the increase in di/dt, the switching speed and the current overshoot increase, resulting in the decrease in T_{rr}, as well as the increase in Q_{rr} obtained by the function $Q_{rr} = \int_0^{T_{rr}} i(t)dt$. The reverse recovery curves at $di/dt = 50$A/μs are shown in the inset. The differences of I_{rrm}, T_{rr} and Q_{rr} for Ga_2O_3 SBD are less than 5% with T from 300 to 500 K, and the curves in the inset of Fig. 4(b) is almost the same, demonstrating the good electronics thermal tolerance improved by the ultrawide bandgap of Ga_2O_3 [1]. This phenomenon also occurs in SiC SBD with high thermal conductivity as shown in Fig. 4(c). However, I_{rrm}, T_{rr}, and Q_{rr} of Si FRD increase significantly as T rises in Fig. 4(d). At $di/dt = 50$ A/μs, T_{rr} and Q_{rr} of Si FRD increase by 66% and 112%, respectively, when T increases from 300 to 400 K because of the lowest E_g value. Table I compares the static and dynamic characteristics of the CT SBD with that of the reported Ga_2O_3 SBDs [4], [11]–[12]. With the large contact dimension, the CT SBD shows low T_{rr} and Q_{rr} owing to the improvement in reverse recovery characteristics by the CT. Since R_{on} decreases and Q_{rr} increases as the active area increases, the FOM = R_{on}·Q_{rr} can reflect the tradeoff between R_{on} and Q_{rr}. The CT SBD obtains the lowest FOM = 0.5 Ω·nC and the highest BFOM = $BV^2/R_{on,sp}$ = 40 MV/cm^2 among the Ga_2O_3 SBDs, and shows comparable FOM to commercial SiC SBD [20]. The BFOM and FOM of the CT SBD can be further improved by thinning the substrate to reduce R_{on} due to the ultralow electron mobility in substrate ($\sim$ 40 cm^2/V·s).

TABLE I
COMPARISON OF Ga_2O_3 AND SiC SBDS AND Si FRD

Devices	D (μm)	I_{rrm} (A)	T_{rr} (ns)	Q_{rr} (nC)	R_{on}·Q_{rr} (Ω·nC)	$BV^2/R_{on,sp}$ (MV/cm^2)
This work	**1000**	**0.22**	**7.5**	**1.0**	**0.5**	**40**
Ga_2O_3 [4]	100	0.038	14.1	0.34	17.3	38
Ga_2O_3 [11]	300	0.42	7.6	~2.0	~8.7	29
Ga_2O_3 [12]	1000	0.7	64	30	85	26
SiC [21]	——	0.32	10	1.8	0.36	——
Si [22]	——	1.43	29	19.0	2.5	——

The rectification characteristics of the β-Ga_2O_3 SBD at different frequencies (f) are shown in Fig. 5(a)–(d). V_{out} curves are shown as half-sine waveforms due to the rectification effect. Fig. 5(e) shows the equivalent circuit to test the rectification characteristics, wherein the packaged large area β-Ga_2O_3 SBD is marked by the red rectangle. R_P, L_P, and C_P framed in the blue rectangle are the parasitic resistance, inductance, and capacitance, respectively, from the cable and test board. When $f \leq 500$ kHz in Fig. 5(a) and (b), the amplitude of V_{out} remain constant and the phase of V_{out} waveform can almost be consistent with that of V_{in} curve, proving the superior rectification characteristics. Because of the parasitic effects from the cable and the test board, V_{out} waveform changes slightly at $f \geq 1$ MHz.

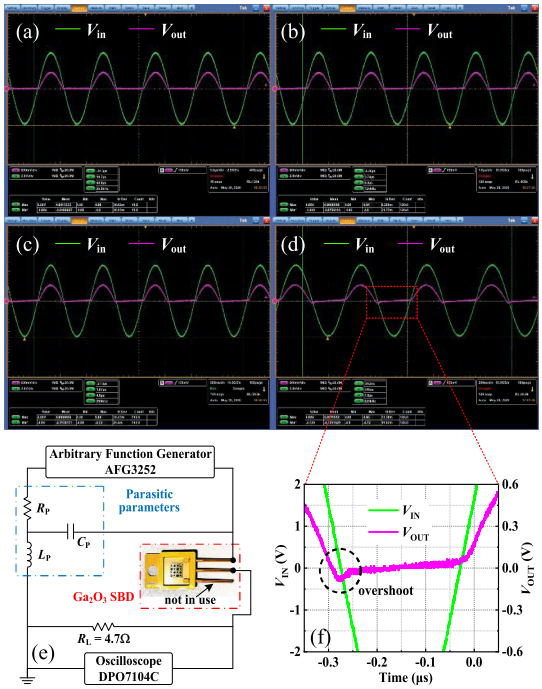

Fig. 5. Rectification characteristics of the Ga_2O_3 SBD measured under (a) $f = 100$ kHz, (b) f=500 kHz, (c) f=1 MHz, and (d) f=2 MHz. (e) Rectification circuit with the packaged Ga_2O_3 SBD. (f) Zoom-in illustration of the figure in the dashed rectangle in Fig. 5(d).

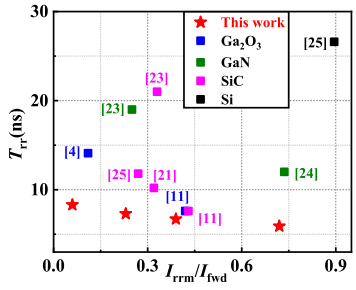

Fig. 6. Plot of T_{rr} versus I_{rrm}/I_{fwd} for this work against several reported SBDs.

The impedance $(\omega C_J)^{-1}$ of the junction capacitance (C_J) decreases as the operation frequency increases. Especially at $f =$ 2 MHz as shown in Fig. 5(f), the output waveform shows the relatively obvious phase shift and overshoot due to the shortened period and the influence of C_J on the high-frequency characteristics, but the rectification capability maintains. The reduction of electron concentration caused by the CT is conducive to the low C_J, which is needed for high-frequency operations and applications. The further reduction in C_J can be achieved by decreasing the doping concentration in epitaxy layer.

The comparison of T_{rr} versus I_{rrm}/I_{fwd} between β-Ga_2O_3 CT SBD and reported Ga_2O_3, GaN, SiC, and Si diodes with similar *BV* [4], [11], [23]–[25] is shown in Fig. 6. The ratio of I_{rrm}/I_{fwd} can reflect the degree of current overshoot. As the *di*/*dt* increases, T_{rr} decreases and I_{rrm} increases at a constant value of I_{fwd}. The fabricated CT SBD simultaneously shows a competitively short reverse recovery time and small reverse recovery current overshoot. It demonstrates that the CT can effectively improve the dynamic characteristics and reliability of the circuit system.

IV. Conclusion

In this letter, a high-performance vertical β-Ga_2O_3 SBD with the CT was fabricated and analyzed. This termination structure is not only effective and easy to implement, but also enables the device to have ultrashort reverse recovery time of 7.5 ns and ultralow reverse recovery charge of 1.0 nC with the *BV* up to 400 V. Moreover, the rectification characteristics were tested by a half-wave rectification circuit. Compared with other reported works, the β-Ga_2O_3 CT SBDs show great advantages in dynamic behavior. The vertical β-Ga_2O_3 SBDs are promising candidates for high power and high-frequency electronic applications.

References

[1] H. Dong *et al.*, "Progress of power field effect transistor based on ultra-wide bandgap Ga_2O_3 semiconductor material," *J. Semicond.*, vol. 40, no. 1, 2019, Art. no. 011802.
[2] A. Kuramata, K. Koshi, S. Watanabe, Y. Yamaoka, T. Masui, and S. Yamakoshi, "High-quality β-Ga_2O_3 single crystals grown by edge-defined film-fed growth," *Jpn. J. Appl. Phys.*, vol. 55, no. 12, 2016, Art. no.1202A2.
[3] M. Higashiwaki and G. H. Jessen, "Guest editorial: The dawn of gallium oxide microelectronics," *Appl. Phys. Lett.*, vol. 112, no. 6, 2018, Art. no. 060401.
[4] X. Lu, X. Zhang, H. Jiang, X. Zou, K. M. Lau, and G. Wang, "Vertical β-Ga_2O_3 Schottky barrier diodes with enhanced breakdown voltage and high switching performance," *Phys. Status Solidi A*, vol. 217, 2020, Art. no. 1900497.
[5] H. Zhou *et al.*, "High-performance vertical β-Ga_2O_3 Schottky barrier diode with implanted edge termination," *IEEE Electron Device Lett.*, vol. 40, no. 11, pp. 1788–1791, Nov. 2019.
[6] Z. Hu *et al.*, "Beveled fluoride plasma treatment for vertical β-Ga_2O_3 Schottky barrier diode with high reverse blocking voltage and low turn-on voltage," *IEEE Electron Device Lett.*, vol. 41, no. 3, pp. 441–444, Mar. 2020.
[7] W. Li, K. Nomoto, Z. Hu, D. Jena, and G. Xing, "Field-plated Ga_2O_3 trench Schottky barrier diodes with a $BV^2/R_{on,sp}$ of up to 0.95 GW/cm^2," *IEEE Electron Device Lett.*, vol. 41, no. 1, pp. 107–110, Jan. 2020.
[8] M. Ji *et al.*, "Demonstration of large-size vertical Ga2O3 Schottky barrier diodes," *IEEE Trans. Power Electron.*, vol. 36, no. 1, pp. 41–44, Jan. 2021.
[9] J. Yang *et al.*, "^{60}Co gamma ray damage in homoepitaxial β-Ga_2O_3 Schottky rectifiers," *ECS J. Solid State Sci. Technol.*, vol. 8, no. 7, pp. Q3041–Q3045, Feb. 2019.
[10] T. Harada and A. Tsukazaki, "Dynamic characteristics of PdCoO2/β-Ga_2O_3 Schottky junctions," *Appl. Phys. Lett.*, vol. 116, no. 23, 2020, Art. no. 232104.
[11] A. Takatsuka *et al.*, "Fast recovery performance of β-Ga_2O_3 trench MOS Schottky barrier diodes," in *Proc. 76th Device Res. Conf.*, 2018, pp. 1–2.
[12] J. Yang *et al.*, "Dynamic switching characteristics of 1 A forward current β-Ga_2O_3 rectifiers," *IEEE J. Electron Device Soc.*, vol. 7, pp. 57–61, Mar. 2019.
[13] R. Lingaparthi *et al.*, " Effects of oxygen annealing of β-Ga_2O_3 epilayers on the properties of vertical Schottky barrier diodes," *J. Solid State Sci. Technol.*, vol. 9, no. 2, Feb. 2020, Art. no. 024004.
[14] Y. Wang *et al.*, "High-voltage (201) β-Ga_2O_3 vertical Schottky barrier diode with thermally-oxidized termination," *IEEE Electron Device Lett.*, vol. 41, no. 1, pp. 131–134, Jan. 2020.
[15] G. Xie *et al.*, "Breakdown-voltage-enhancement technique for RF-based AlGaN/GaN HEMTs with a source-connected air-bridge field plate," *IEEE Electron Device Lett.*, vol. 33, no. 5, pp. 670–672, Jan. 2012.
[16] B. Shankar, A. Soni and M. Shrivastava, "Electro-thermo-mechanical reliability of recessed barrier AlGaN/GaN Schottky diodes under pulse switching conditions," *IEEE Trans. Electron Devices*, vol. 67, no. 5, pp. 2044–2051, May 2020.

[17] A. Jayawardena, A. C. Ahyi, and S. Dhar, "Analysis of temperature dependent forward characteristics of Ni/(01)-Ga_2O_3 Schottky diodes," *Semicond. Sci. Technol.*, vol. 31, no. 11, Sep. 2016, Art. no. 115002.

[18] Z. Jian, S. Mohanty, and E. Ahmadi, "Temperature-dependent current-voltage characteristics of β-Ga_2O_3 trench Schottky barrier diodes," *Appl. Phys. Lett.*, vol. 116, no. 15, 2020, Art. no. 152104.

[19] D. Cimmino and S. Ferrero, " High-voltage temperature humidity bias test (HV-THB): Overview of current test methodologies and reliability performances," *Electronics*, vol. 9, no. 11, Nov. 2020, Art. no. 1884.

[20] R. Potera, T. Witt, and Y. Zheng, "Analysis of transient HTRB leakage in a SiC field ring termination," in *Proc. IEEE Int. Rel. Phys. Symp.*, 2020, pp. 1–5, doi: 10.1109/IRPS45951.2020.9129571.

[21] *Commercial SiC Diode (Rec Schottky)_Part Number: STPSC406*. Geneva, Switzerland: STMicroelectronics Co., 1987.

[22] *CommercialSi Diode (Superfast Diode)_Part Number: SF36*. Shanghai, China: MIC electronic Co. LTD, 1988.

[23] S. Han, S. Yang, R. Li, X. Wu, and K. Sheng, "Current-collapse-free and fast reverse recovery performance in vertical GaN-on-GaN Schottky barrier diode," *IEEE Trans. Power Electron.*, vol. 34, no. 6, pp. 5012–5018, Jun. 2019.

[24] K. Hsueh, H. Chiu, H. Wang, H. Kao, F. Chien, and W. Lin, "The demonstration of recessed anodes AlGaN/GaN Schottky barrier diodes using microwave cyclic plasma oxidation/wet etching techniques," *Jpn. J. Appl. Phys.*, vol. 58, no. 7, 2019, Art. no. 071002.

[25] J.-H. Lee, C. Park, K.-S. Im, and J.-H. Lee, "AlGaN/GaN-based lateral type Schottky barrier diode with very low reverse recovery charge at high temperature," *IEEE Trans. Electron Devices*, vol. 60, no. 10, pp. 3032–3039, Oct. 2013.